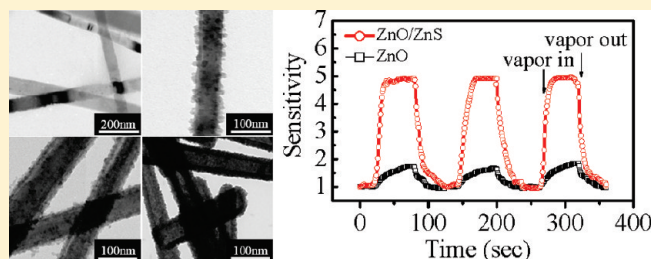


A Facile Chemical Conversion Synthesis of ZnO/ZnS Core/Shell Nanorods and Diverse Metal Sulfide Nanotubes

X. M. Shuai and W. Z. Shen*

Laboratory of Condensed Matter Spectroscopy and Opto-Electronic Physics, and Key Laboratory of Artificial Structures and Quantum Control (Ministry of Education), Department of Physics, Shanghai Jiao Tong University, 800 Dong Chuan Road, Shanghai 200240, China

ABSTRACT: We report a simple chemical conversion approach to fabricate ZnO/ZnS core/shell nanorods and various metal sulfide nanotubes such as ZnS, Ag₂S, CuS, PbS, and Bi₂S₃. The formation mechanisms of the ZnO/ZnS core/shell nanorods and ZnS nanotubes are due to the sulfidation conversion and the Kirkendall effect, respectively, in a low-temperature hydrothermal growth through the reaction of ZnO nanowires and thioacetamide. The successful chemical conversion of the ZnS nanotubes into the other metal sulfide nanotubes is to utilize the large difference in solubility between ZnS and the other metal sulfides for the effective transformation. In addition to the perfect maintenance of the morphology after conversion, we have shown that the yielded metal sulfide nanostructures possess good crystalline qualities with high optical and sensing performances. The present chemical conversion technique is expected to be employed in a broad range of applications to fabricate innovative semiconductor core/shell and hollow structures with various compositions and shapes for unique properties.



1. INTRODUCTION

In recent years, considerable effort has been devoted to the design and controlled fabrication of core/shell structured materials as well as hollow structures in physics, chemistry, and material science communities due to their specific structures and unique properties.^{1–11} The core/shell structured materials usually demonstrate an improvement in physical and chemical properties for electronics, magnetism, optics, catalysis, mechanics, and others.^{1–7} Hollow nanomaterials possess the unique properties of special hollow geometrical shapes, low density, high specific surface area, and distinct optical properties, showing great potential in many fields, including solar cells, catalysts, sensors, photonic crystals, nanoscale chemical reactors, energy-storage media, and drug-delivery carriers.^{8–11} Over the past decade, there have been immense efforts to fabricate a variety of core/shell and hollow structures, such as noble-metal, hydroxide, semiconductor, organic, and inorganic materials with tailored structural, optical, and surface properties.^{12–24} Particularly, scientific and technological interests have been considered to the semiconductor metal sulfide core/shell nanorods and nanotubes, as well as their potential applications.^{21–24}

So far, among various strategies for synthesizing semiconductor core/shell nanorods and nanotubes, the template-based techniques turn out to be a powerful method, where the widely employed templates include carbon nanotubes, inorganic–organic composite nanowires, and anodic aluminum oxide membranes.^{25–27} However, the template-assisted approach always requires extremely complicated synthetic procedures and increases the production cost.²⁸ In addition, removal of the template has also increased the complexity of the process and

inevitably affects the purity of the materials.²⁹ Therefore, it is desirable to develop a facile, versatile synthetic pathway to fabricate semiconductor metal sulfide core/shell nanorods and nanotubes of various compositions. In fact, chemical conversion and cation exchange have been demonstrated as effective ways to convert the chemical compositions of nanostructures without destroying the original morphology.³⁰ Our previous studies on the transformation of composition in the core/shell microspheres (from ZnO/ZnS to ZnO/Ag₂S and ZnO/CuS)³¹ and in the hollow microspheres (from ZnS to other various metal sulfides)³² have indicated the significance of chemical conversion and cation exchange. Nevertheless, little has been devoted to the development of a general and low-cost synthetic method to realize the conversion from one kind of semiconductor metal sulfide nanorods/nanotubes to others to broaden their potential applications.

In this Article, we demonstrate the successful fabrication of ZnO/ZnS core/shell nanorods and ZnS nanotubes by conversion from ZnO nanowires via hydrothermal process at low temperatures. We have further realized the first synthesis of various metal sulfide nanotubes (Ag₂S, CuS, PbS, and Bi₂S₃) transformed from the ZnS nanotubes. The key point of the method is to utilize the large difference in solubility between ZnS and the other metal sulfides for the effective transformation. On the basis of the structural, morphological, and systematic optical investigation, we have proposed the preliminary growth

Received: January 19, 2011

Revised: March 4, 2011

Published: March 18, 2011

mechanism. Moreover, in comparison with ZnO nanowires, enhanced ultraviolet (UV) emission and superior properties of ZnO/ZnS heteronanorods have been observed and explained from the passivated nonradiative recombination sites²¹ and improved conductance variation^{33,34} points of view, respectively. The presented strategy is effective and economic with the advantages of simplicity (without any special equipments or templates), low growth temperature (90 °C), and high yield (near 100% morphological yield), and can be developed as a general method to fabricate functional semiconductor core/shell and hollow structures with various compositions and shapes for unique properties.

2. EXPERIMENTAL SECTION

Synthesis of ZnO Nanowires. In a typical experiment, 0.2 g of ZnCl₂ and 20 g of Na₂CO₃ were added into a 50 mL Teflon-lined stainless steel autoclave and filled with distilled water up to 90% of its volume. After vigorous stirring for 30 min, the autoclave was maintained at 140 °C for 12 h, followed by cooling naturally to room temperature. Finally, ZnO nanowires were obtained as a white powdery product after systematic centrifuging and cleaning.

Synthesis of ZnO/ZnS Core/Shell Structured Nanorods and ZnS Nanotubes. Silicon or glass slide substrates with ZnO nanowires on them were transferred into a Pyrex glass bottle containing 0.2 M thioacetamide (TAA) aqueous solution. The sulfidation was carried out at 90 °C for 1–9 h in a conventional laboratory oven. The final products on the substrates were washed with deionized water repeatedly to remove the possible impurities and then dried at room temperature.

Synthesis of Other Metal Sulfide Nanotubes. Synthesis of other metal sulfide nanotubes was achieved by a chemical conversion process using the prefabricated ZnS nanotubes on silicon or quartz substrates as sacrificial templates. In a typical synthesis of Ag₂S, PbS, CuS, and Bi₂S₃ nanotubes, the aqueous solutions used were 50 mM AgNO₃, 50 mM Pb(NO₃)₃, 100 mM Cu(NO₃)₂, and 100 mM Bi(NO₃)₃, respectively. To the latter two solutions was also added 70 mM tartaric acid because Cu⁺ and Bi⁺ are apt to hydrolyze in water. After treating at 90 °C for proper times, the final products on the substrates were washed thoroughly using deionized water to remove any coprecipitated salts and then dried in air at 50 °C.

Characterization. The general morphology of the products was characterized by field-emission scanning electron microscopy (FE-SEM, Philips XL30FEG) with an accelerating voltage of 5 kV and a high-resolution transmission electron microscopy (HRTEM; JEOL JEM-2100F). Energy dispersive X-ray (EDX) analysis was also performed during the FE-SEM observation, and the selected area electron diffraction (SAED) was processed during HRTEM measurements. The crystal structure and composition of the samples were characterized by X-ray diffraction (XRD, D/max-2200/PC) with high intensity Cu K α radiation ($\lambda = 1.5418 \text{ \AA}$). Raman and photoluminescence (PL) spectra were measured at room temperature on a Jobin Yvon LabRAM HR 800UV micro-Raman/PL system. Raman spectra were recorded at the backscattering configuration under the excitation of a He–Cd laser (325.0 nm) for ZnO nanowires, ZnO/ZnS core/shell nanorods (6 h), ZnS nanotubes, as well as Ag₂S nanotubes, but Ar⁺ laser (514.5 nm) was used for the other metal sulfides. PL spectra of ZnO nanowires, ZnO/ZnS core/shell nanorods (6 h), and ZnS nanotubes were taken under the He–Cd laser excitation.

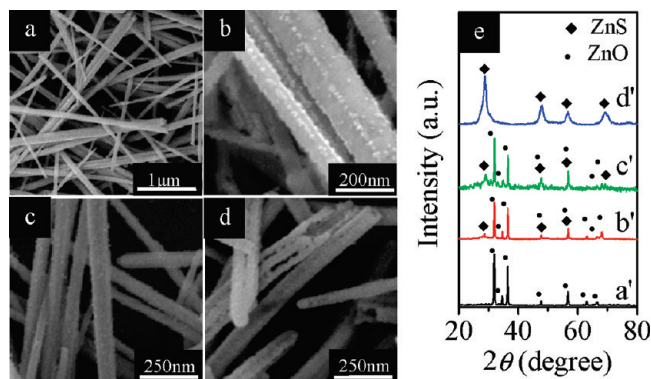


Figure 1. FE-SEM images of (a) ZnO nanowires; (b) ZnO/ZnS core/shell nanorods, 1 h; (c) ZnO/ZnS core/shell nanorods, 6 h; and (d) ZnS nanotubes, 9 h. (e) The corresponding XRD of initial ZnO nanowires, ZnO/ZnS core/shell nanorods (1 and 6 h), and pure ZnS nanotubes.

Sensing Property Measurements. For fabricating gas sensors of the ZnO nanowires and ZnO/ZnS core/shell nanorods (6 h), the as-prepared products were dispersed into a certain amount of ethanol to form a paste, then were coated onto a ceramic tube (the coating thickness is about 0.25 mm) on which a pair of gold electrodes was previously printed. A Ni–Cr alloy was inserted into the ceramic tube to provide the operating temperature. The gas sensors were dried and aged for 10 days before the first measurement to improve their stability. Measurements on gas response have been performed with a static test system (HW-30A) made by Henan Hanwei Electronics Co. Ltd., China. Detecting gas, such as H₂S, was injected into a test chamber and mixed with air. With this measuring system, the steady-state value of resistance can be reached, and the sensor response is repeatable over time. The gas sensitivity (response magnitude) in this Article was defined as $S = G_{\text{gas}}/G_{\text{air}}$, where G_{gas} and G_{air} were the conductances of a sensor in a test gas and in air, respectively. The working temperature is kept at 350 °C during the test process.

3. RESULTS AND DISCUSSION

Structural and Compositional Characterization of ZnO Nanowires, ZnO/ZnS Core/Shell Nanorods, and ZnS Nanotubes. In our experiments, ZnO nanowires were first prepared by a hydrothermal process. Figure 1a shows the FE-SEM image of the as-prepared nanowires; their diameters are about 70–100 nm with an aspect ratio over 150. In the following, to realize ZnO/ZnS core/shell nanorods and ZnS nanotubes, we transfer the silicon or glass slide substrates with ZnO nanowires on them into a solution containing 0.2 M TAA. In the reaction system, TAA as S source hydrolyzes and releases H₂S under 90 °C, and then H₂S reacts with ZnO at the interface of nanowires to form ZnS.²³ Figure 1b,c presents the FE-SEM images of two samples obtained at different sulfidation times (1 and 6 h). If the sulfidation time is very short (1 h), some ZnS nanoparticles on the ZnO nanowires were observed because ions exchange happens as S²⁻ reacts with Zn²⁺ slowly dissolved from the surface of ZnO nanowires to form initial ZnS shells, as depicted in Figure 1b. As the sulfidation time is increased to 6 h, the ZnS shells become thicker as more and more ZnS nanoparticles pile up on the initial ZnS shells, and the shells are robust enough to form ZnO/ZnS core/shell nanorods (Figure 1c).

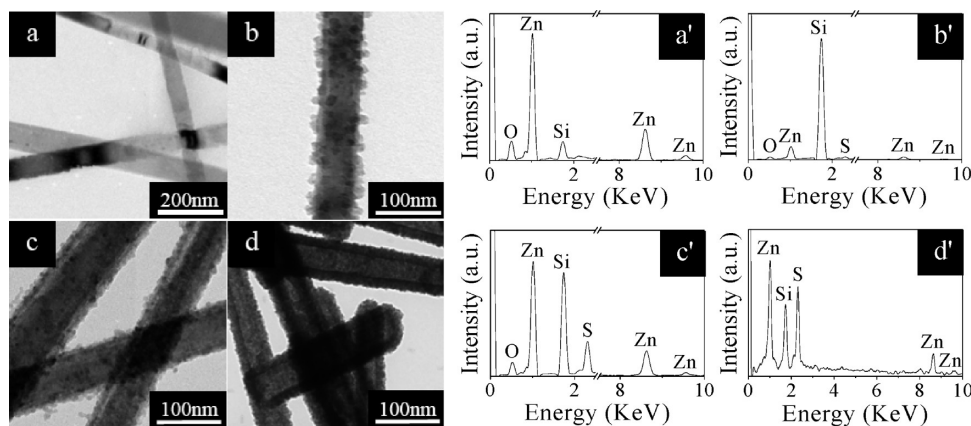


Figure 2. TEM images of (a) ZnO nanowires; (b) ZnO/ZnS core/shell nanorods, 1 h; (c) ZnO/ZnS core/shell nanorods, 6 h; and (d) ZnS nanotubes, 9 h. The corresponding EDX of (a') initial ZnO nanowires, (b' and c') ZnO/ZnS core/shell nanorods with two different reaction times, and (d') pure ZnS nanotubes.

Finally, when further prolonging the sulfidation time to 9 h under hydrothermal conditions, all ZnO nanowires change to ZnS nanotubes. Figure 1d shows the FE-SEM image of the obtained ZnS nanotubes. One can see that some of the shells have an irregular open tip, clearly demonstrating the hollow nature of the prepared nanotubes. The formation mechanism of the ZnS nanotubes can be explained by the Kirkendall process, which normally refers to comparative diffusive migrations among different atomic species in metals and/or alloys under thermally activated conditions.³⁵

The corresponding XRD patterns in Figure 1e give clear evidence for the FE-SEM observation of the samples obtained through various reaction times. From curve a', the typical diffraction peaks of hexagonal ZnO structure (PDF no. 36-1451) indicate that the nanowires consist of pure single-crystalline ZnO before reacting with TAA solution. When the reaction time is 1 h, the diffraction peak of ZnO is still very strong with a very weak peak of cubic ZnS (PDF no. 05-0566), as demonstrated in curve b'. As the sulfidation time is increased to 6 h, the ratio of the characterization peaks of ZnS/ZnO increases (curve c'), implying that more and more ZnO was changed into ZnS with the reaction time increasing. While the sulfidation time is up to 9 h, all of the XRD characterization peaks of ZnO disappear. Only the diffraction peak of ZnS can be found in the XRD pattern of the final product (curve d'), demonstrating that all of the ZnO nanowires were converted into ZnS nanotubes.

We have further investigated the crystal structures and chemical compositions of the as-prepared products by TEM and EDX techniques. Figure 2a shows the TEM image of the initial ZnO nanowires, where the prepared ZnO nanowires appear to be smooth on the surface. Figure 2b presents the TEM image of ZnO/ZnS core/shell nanorods obtained at 1 h. One can notice that the outer layers were composed of nanoparticles with a mean size of 18 nm. With the increase of the sulfidation reaction time to 6 h, the TEM in Figure 2c reveals that every nanorod was formed with a solid core and a shell. The apparent contrast between the inner core and the outer shell suggests the existence of a core/shell structure. Figure 2d is a representative TEM image of the obtained ZnS nanotubes. The strong contrast difference in the nanotubes with a light inner center and a relative dark edge confirms that the yielded ZnS nanotubes are all hollow. The diameter of the nanotubes is about 70 nm with a shell as thick as

16–20 nm. It is also noticed that these products are shorter in length as compared to ZnO nanowire precursors while the diameter is nearly the same, indicating that ZnO nanowires have broken into smaller sections during the chemical conversion process.

Accordingly, the EDX spectrum of ZnO nanowires, shown in Figure 2a', indicates that the obtained nanowires are composed of only Zn and O elements. The signal of Si originates from the substrate. After the sulfidation reaction in TAA, we can observe the successful incorporation of S element into the ZnO nanowires in the compositional information of the EDX spectrum in Figure 2b', and the S/O stoichiometric ratio becomes quite high with the increase of the reaction time shown in Figure 2c', where Zn, O, and S were the primary elements due to the fact that more and more O atoms were replaced by S atoms with the sulfidation reaction processing. Further sulfidation reaction will yield pure ZnS nanotubes, which can be unambiguously confirmed by the EDX spectrum in Figure 2d'. There are only Zn, S, and Si elements without any O element.

HRTEM observation can give deep insight into the structural features of the as-prepared products. Figure 3a presents the TEM image of a well-developed ZnO nanowire with width of 70 nm. The typical HRTEM image, recorded from a certain nanowire, is shown in Figure 3a', where the crystal lattice fringes are clearly observed and the average distance between the adjacent lattice planes is 0.256 nm, corresponding to the (0002) plane lattice distance of hexagonal-structured ZnO. This observation demonstrates that ZnO nanowires prepared in the present method grow along [0001] direction. The SAED pattern of the nanowire (inset of Figure 3a') also proves its single crystal nature and growth direction along *c*-axis. Figure 3b displays the TEM image of the ZnO/ZnS nanorods obtained by sulfidation time of 6 h, where the core/shell structure can be clearly observed. The HRTEM investigations (Figure 3b') of an individual ZnO/ZnS nanorod taken at the marked region of Figure 3b show that another set of lattice planes were formed on the surface, revealing the polycrystalline nature of the ZnS shell. The corresponding SAED pattern (inset in Figure 3b') exhibits a spotted pattern that corresponds to the ZnO single crystal, and a set of diffraction rings that are consistent with the polycrystalline ZnS nanoparticles, confirming the core/shell structure. Figure 3c is a representative TEM image of the as-prepared ZnS nanotube obtained

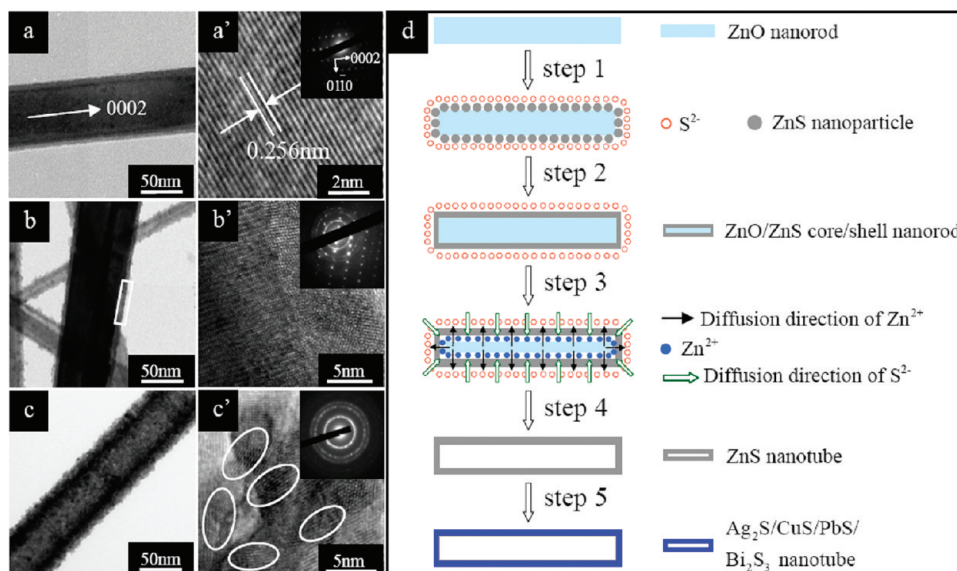


Figure 3. TEM images of (a) ZnO nanowire, (b) ZnO/ZnS core/shell nanorods, 6 h, and (c) ZnS nanotube, 9 h. HRTEM images of (a') ZnO nanowire, (b') ZnO/ZnS core/shell nanorods, 6 h, and (c') ZnS nanotube, 9 h, together with the corresponding SAED patterns shown in the insets. (d) Schematic illustration of growth mechanism of ZnO/ZnS core/shell nanorods, ZnS, Ag_2S , CuS, PbS, and Bi_2S_3 nanotubes.

at sulfidation time of 9 h. Figure 3c' presents a HRTEM image taken on the edge of the ZnS nanotube; only polycrystalline nature of ZnS nanotubes can be observed. The inset of Figure 3c' is the corresponding ring-like SAED pattern without spotted pattern taken on a single nanotube, also providing evidence for the polycrystalline nature of ZnS nanotubes. The diffraction rings can be outward indexed to (111), (220), and (311) crystal planes of the cubic ZnS, respectively.^{24,31}

According to the experimental results described above, we propose the possible formation mechanism of ZnO/ZnS core/shell nanorods and ZnS nanotubes as illustrated in Figure 3d. At the beginning of sulfidation reaction of ZnO nanowires in TAA, S^{2-} released from the decomposition of TAA reacts with the Zn^{2+} slowly dissolved from the surface of ZnO nanowires to produce ZnS nanoparticles around the ZnO wires. A nonuniform shell composed of ZnS nanoparticles is formed gradually surrounding the ZnO core (step 1). As the sulfidation time is increased, more and more ZnS nanoparticles are produced and piled up to form a uniform and dense ZnS shell, leading to the formation of ZnO/ZnS core/shell nanorods, as shown in step 2. With the further sulfidation reaction processing, the ZnS shell separates the inner ZnO core from the outer sulfur ion and prevents further direct chemical reaction between the two reactants, which induces the concentration gradient of Zn^{2+} and S^{2-} from the solution outside the ZnS shell to the surface of the ZnO core inside the shell. Under the driving force of the concentration gradient, the Zn^{2+} will diffuse outward through the ZnS shell to its outside, while the S^{2-} in the solution will diffuse inward through the ZnS shell to its inside surface (step 3). According to the Kirkendall effect, the outward transport rate of Zn^{2+} is much faster than the inward transport rate of S^{2-} species through the formed ZnS shell,⁸ and a gap is gradually formed between the ZnO core and the ZnS shell. As a result, the size of ZnO core will become smaller and smaller due to the consuming of inside Zn^{2+} , and the ZnO/ZnS core/shell structures will completely transform to ZnS nanotubes when the reaction time reaches 9 h (step 4). We notice that a process analogous to the

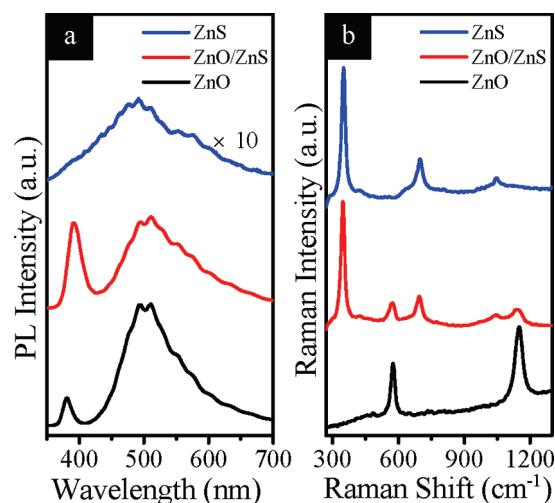


Figure 4. Room-temperature (a) PL and (b) Raman spectra of ZnO nanowires, ZnO/ZnS core/shell nanorods, 6 h, and ZnS nanotubes, 9 h.

Kirkendall phenomenon has been successfully developed recently for nanoscale fabrication of a variety of hollow crystals.^{9–11} Other metal sulfide (Ag_2S , CuS, PbS, and Bi_2S_3) nanotubes can be further synthesized after treating the prepared ZnS nanotubes in solutions containing the corresponding metal cations by a simple chemical conversion technique³² utilizing the large difference in solubility between ZnS and other metal sulfides (step 5). We will describe this transformation in detail later.

Optical Properties of ZnO Nanowires, ZnO/ZnS Core/Shell Nanorods, and ZnS Nanotubes. To investigate the optical properties of these novel semiconductor nanostructures, we have performed room-temperature PL and Raman scattering measurements. Figure 4a presents the PL spectra of the initial ZnO nanowires, ZnO/ZnS core/shell nanorods sulfidation for 6 h, and ZnS nanotubes obtained at 9 h. Two emitting bands, including a narrow UV emission peak at 380 nm along with a

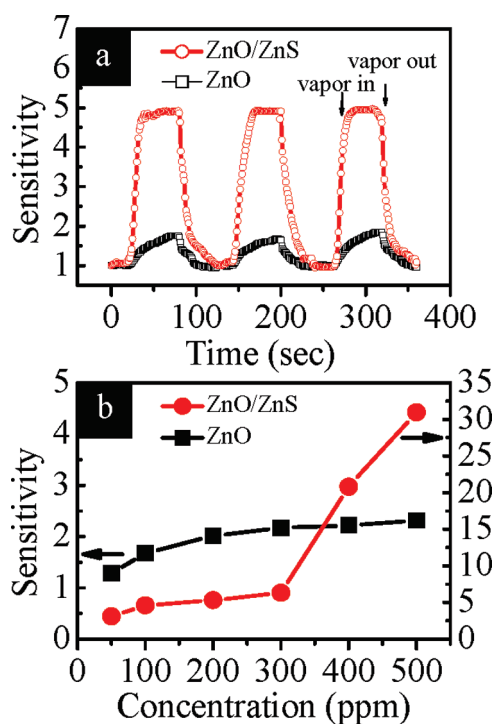


Figure 5. (a) Response of ZnO nanowires and ZnO/ZnS core/shell nanorods (6 h) to 100 ppm H₂S vapor in air. (b) H₂S-sensing properties of ZnO nanowires and ZnO/ZnS core/shell (6 h) nanorods at various concentrations of H₂S vapor in air. Working temperature is 350 °C.

broad green emission centered around 502 nm, have been observed in ZnO nanowires. It is reported that the UV emission originates from the recombination of free excitons in the near-band edge of the wide band gap ZnO, and the broad visible luminescence has commonly been attributed to the singly ionized oxygen vacancy in ZnO and results from the recombination of a photogenerated hole with the single ionized charged state of the defect.^{36–38} The PL spectrum of ZnO/ZnS core/shell nanorods shows a distinctly enhanced UV emission with a small red-shift (about 12 nm) and a reduced green emission, as compared to that of pure ZnO nanowires. The red-shift of the UV emission can be attributed to the strain caused by the lattice mismatch between ZnO and ZnS. Theoretical work has already predicted that the strain in the ZnO/ZnS interface is strong enough to reduce the total system band gap.³⁹ Moreover, a wider band gap semiconductor material (ZnS) coated on the ZnO passivates the surface electronic states of the ZnO cores, resulting in an obvious enhancement in the UV luminescence. Such an enhancement in the emission has also been observed in the coaxial CdS/ZnS nanowires.²¹ In contrast, the PL spectrum of ZnS nanotubes exhibits only a broad weak peak centered at about 492 nm, similar to the reported PL characteristics of other ZnS nanostructures.^{40,41} The periodic ripples are due to the interferometer effect from the filter in the experimental system. From the above observation, we can conclude that the intensity of UV emission was obviously enhanced after a thin layer of ZnS was coated on ZnO nanowires. Therefore, these ZnO/ZnS core/shell nanorods are more applicable for the fabrication of optoelectronic devices, such as UV light-emitting diodes and diode lasers.

Figure 4b shows the corresponding Raman spectra of these three typical samples, which give further evidence for the crystallization,

structural disorder, and defects. We have observed two strong peaks centered at 575 and 1150 cm⁻¹ for ZnO nanowires, which can be attributed to the A₁[longitudinal optical (LO)] and A₁(2LO) phonon modes, respectively,⁴² indicating that the ZnO nanowires are of fine quality. In addition to the A₁(LO) and A₁(2LO) phonon modes of ZnO, there are three other Raman peaks in the ZnO/ZnS nanorods synthesized after sulfidation time of 6 h. The Raman peaks located at 350, 699, and 1045 cm⁻¹ correspond well to the first-, second-, and third-order LO phonon modes in ZnS, respectively,⁴³ demonstrating the formation of the core/shell structure. Clearly, the Raman spectrum of ZnS nanotubes obtained at 9 h shows only the three resonant Raman peaks at 350, 699, and 1045 cm⁻¹, revealing that all of the ZnO nanowires have been converted into ZnS nanotubes. The observation of multiple resonant Raman peaks indicates that the yielded ZnS nanotubes possess good optical quality.⁴² This is also confirmed by the fact that there are few defects on the surface of the ZnS nanotubes, because we cannot detect any peaks corresponding to the surface optical phonon modes in the Raman spectrum.⁴⁴

Hydrogen Sulfide-Sensing Properties of the ZnO/ZnS Core/Shell Nanorods. It is well-known that H₂S is a toxic and flammable gas, which is badly harmful to the human body and the environment. The detection of H₂S is very crucial to protect human health and environmental safety. We show in Figure 5a the response of ZnO/ZnS core/shell nanorods to 100 ppm H₂S vapor in air at an operating temperature of 350 °C. For comparison, we also present the response curve of uncoated ZnO nanowires measured at the same conditions. From the real-time responses toward H₂S, the sensitivities ($S = G_{\text{gas}}/G_{\text{air}}$) of ZnO nanowires and ZnO/ZnS core/shell nanorods increase obviously as the target gas is injected, and the sensitivities return back to the initial state when the detected gas is released by dry air flow, as marked in Figure 5a. In contrast, the sensitivity of ZnO/ZnS core/shell nanorods reaches 5.0 for 100 ppm H₂S, which is much higher than that of ZnO nanowires (1.7). The responses of ZnO nanowires and ZnO/ZnS core/shell nanorods sensors to H₂S vapor (350 °C) are depicted in Figure 5b as a function of gas concentration. It is found that, at any concentration of H₂S vapor, the ZnO/ZnS core/shell nanorods have a much higher sensitivity than do the uncoated ZnO nanowires. The response of ZnO/ZnS core/shell nanorods sensing to 500 ppm H₂S gas is more than 14 times larger than that of ZnO nanowires. Clearly, the ZnO/ZnS core/shell nanorods feature an improved H₂S-sensing performance such as high sensitivity as compared to the uncoated ZnO nanowires.

The mechanism of the ZnO-based gas sensors has been discussed since 1979, and the most widely accepted model is based on the modulation of the depletion layer by oxygen adsorption.^{45,46} Oxygen from the ambient adsorbs on the exposed surface of ZnO, extracts an electron from the ZnO conduction band, and ionizes to O⁻ or O²⁻ (O⁻ is believed to be dominant).⁴⁵ Consequently, depletion layers are formed in the surface area of ZnO, causing the carrier concentration and electron mobility (due to scattering) to decrease. When exposed to such reducing gases as H₂S, the H₂S molecules will react with the adsorbed O⁻, releasing the trapped electron back to the conduction band, and then both the carrier concentration and the carrier mobility of ZnO increase. Such a variation in the conductance of ZnO can be used to detect both reducing and oxidizing gases,⁴⁶ and the gas sensitivity of a ZnO sensor can be improved by enhancing its conductance variation. Recently, the

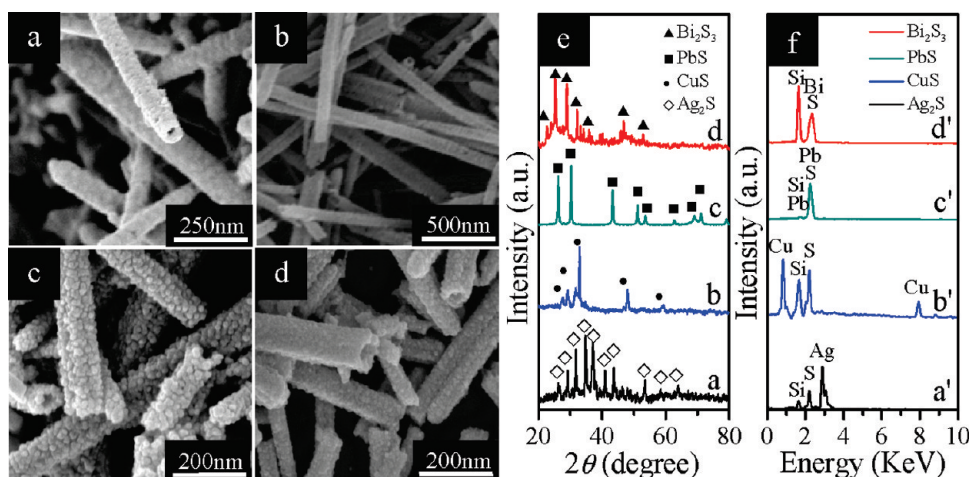


Figure 6. FE-SEM images of (a) Ag_2S , (b) CuS , (c) PbS , and (d) Bi_2S_3 nanotubes. The corresponding (e) XRD and (f) EDX of Ag_2S , CuS , PbS , and Bi_2S_3 nanotubes.

adsorption–desorption process of oxygen has also been found to occur on the surfaces of ZnS nanostructures.³³ Thus, the advantages of the ZnO/ZnS core/shell structures are 2-fold. On the one hand, oxygen molecules in air should deplete electrons in both ZnO core and ZnS shell. On the other hand, electrons may be scattered by the interface between ZnO and ZnS in ZnO/ZnS heterostructure.³⁴ A high electric resistance in air is therefore expected in ZnO/ZnS core/shell nanorods. As exposed to H_2S vapor, the H_2S reacts with the adsorbed oxygen species, and the extracted electrons can be released from both ZnO core and ZnS shell, resulting in a much improved sensitivity of the ZnO/ZnS core/shell nanorods (Figure 5), as compared to that of bare ZnO nanowires.

Structural and Compositional Characterization of Ag_2S , CuS , PbS , and Bi_2S_3 Nanotubes. Here, we show the realization of various metal sulfide nanotubes transformed from the ZnS nanotubes. As the first example, Ag_2S nanotubes were successfully synthesized by transferring ZnS nanotubes into aqueous silver nitrate solution for 30 min at 90 °C. Figure 6a shows the FE-SEM image of the as-prepared products; there are no significant morphological changes as compared to ZnS nanotubes (Figure 1d), confirming the realization of morphology transfer from ZnS nanotubes to the others. XRD measurements have been carried out to identify the composition and to analyze the crystalline properties of the prepared samples. Curve a in Figure 6e shows that only diffraction peaks originating from monoclinic Ag_2S (PDF no. 14-0072) are detected, demonstrating that the ZnS (PDF no. 05-0566) nanotubes have been completely converted into Ag_2S ones. The EDX spectroscopy was also introduced to analyze its chemical composition (curve a' in Figure 6f), from which we note that there are only Ag, S, and Si elements without any Zn element, further confirming the total transformation from ZnS to Ag_2S .

We propose the conversion mechanism as follows. Once the obtained ZnS nanotubes were transferred into silver nitrate solution, cation exchange began at the interfaces between the ZnS nanotube surfaces and solution. With the increase in the reaction time, Zn^{2+} was gradually substituted by Ag^+ , resulting in Ag_2S nanotubes. The driving force for the cation exchange is provided by the large difference in solubility between ZnS and Ag_2S [solubility product constant (K_{sp}) of ZnS is 2.93×10^{-25} , whereas K_{sp} of Ag_2S is 6.69×10^{-50}].⁴⁷ The above conversion mechanism reveals that the ZnS nanotubes can act as both

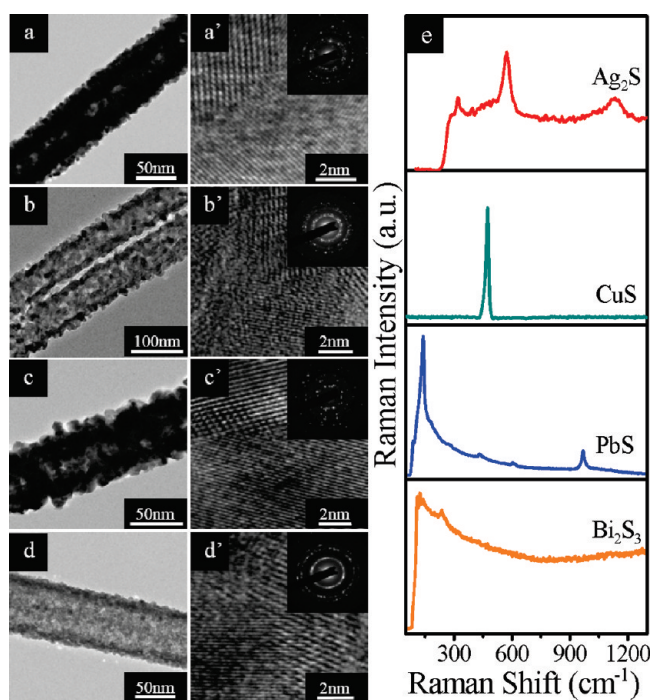


Figure 7. TEM images of (a) Ag_2S , (b) CuS , (c) PbS , and (d) Bi_2S_3 nanotubes. HRTEM images of (a') Ag_2S , (b') CuS , (c') PbS , and (d') Bi_2S_3 nanotubes, together with the corresponding SAED patterns shown in the insets. (e) Room-temperature Raman spectra of the synthesized metal sulfide nanotubes.

reactants and templates during the cation exchange process. We have extended successfully this chemical conversion approach to synthesize the other metal sulfide (such as CuS , PbS , and Bi_2S_3) nanotubes under the condition that those yielded metal sulfides have lower K_{sp} values than that of ZnS by transferring the ZnS nanotubes into solutions containing the corresponding metal cations. Figure 6b–d shows the FE-SEM images of these yielded metal sulfide nanotubes, where the morphologies of the ZnS nanotubes are all preserved during the cation exchange process and the hollow nature of these

nanotubes is clearly evidenced by the irregular open tips of the obtained nanotubes. XRD measurements have been performed to identify the microstructural transformation (Figure 6e). It is found that all diffraction peaks are consistent with the corresponding metal sulfides (CuS, PDF no. 06-0464; PbS, PDF no. 65-9496; and Bi₂S₃, PDF no. 65-2435). EDX spectra have also been provided to check the chemical compositions of the yielded metal sulfide nanotubes (Figure 6f). No impurities are detected in any of these samples, further demonstrating the successful transformations from ZnS nanotubes to the other metal sulfide nanotubes. Therefore, a facile and versatile method has been proposed and realized to synthesize metal sulfide nanotubes.

Figure 7a–d shows TEM images of as-obtained metal sulfide (Ag₂S, CuS, PbS, and Bi₂S₃) nanotubes, showing that these produced samples have uniform tube-like morphology with diameters of 70–75 nm and shells as thick as about 10–30 nm. These metal sulfide nanotubes apparently consist of tiny primary nanocrystallites, indicating a polycrystalline nature of the nanotubes. HRTEM analysis provides further insight into the structures of those nanotubes. Figure 7a'–d' presents the HRTEM images taken on the edge of the metal sulfide nanotubes, which display many nanocrystallites with clear lattice fringes. The corresponding SAED patterns shown in the insets also confirm the polycrystalline feature of these nanotubes, consistent well with the HRTEM observation. The SAED pattern (inset in Figure 7c') of PbS nanotubes exhibits indistinct polycrystalline diffraction rings, which may be due to the larger diameter of the nanocrystallites.

Raman Properties of Ag₂S, CuS, PbS, and Bi₂S₃ Nanotubes. Raman spectroscopy is an effective method for materials structure investigation. However, there is little workup until now reported on the application of Raman characterization for metal sulfide nanotubes. Figure 7e shows the room-temperature Raman spectra of the yielded metal sulfide nanotubes recorded between 50 and 1300 cm⁻¹. The Raman spectrum of the Ag₂S nanotubes exhibits three distinct vibrational peaks at about 320, 573, and 1135 cm⁻¹, which are similar to the previously reported results for Ag₂S hollow microspheres.³² A strong and sharp band at 474 cm⁻¹ in CuS nanotubes, revealing that the lattice atoms are aligned in the periodic array, agrees well with the observation for CuS thin films by Sukarova.⁴⁸ The Raman spectrum of the PbS nanotubes indicates seven bands in the range of 50–1300 cm⁻¹, located at around 90, 139, 174, 274, 433, 600, and 970 cm⁻¹. The peak at ~90 cm⁻¹ resembles a confined transversal optical mode,⁴⁹ while the strong band centered at 139 cm⁻¹ originates from the combination of longitudinal and transversal acoustic modes.⁵⁰ The weak band at ~174 cm⁻¹ is attributed to the fundamental LO phonon mode^{49–52} and those at 433 and 600 cm⁻¹ to its first and second overtones (2LO and 3LO), respectively.^{49,50} It was reported that the small peak at ~274 cm⁻¹ was due to two-phonon processes in PbS nanocrystals.⁵¹ The band centered at 970 cm⁻¹ is consistent with the reported values for PbS dendritic structures.⁵³ The Raman spectrum of the Bi₂S₃ nanotubes contains bands at about 110, 123, 139, and 237 cm⁻¹. These lattice vibrations at 110, 123, 139, and 237 cm⁻¹ may all be related to the surface phonon modes, in accord with the previously reported results in Bi₂S₃ nanowires,⁵⁴ nanorods,⁵⁵ and thin films.⁵⁶

4. CONCLUSIONS

In summary, ZnO/ZnS core/shell nanorods and ZnS nanotubes have been successfully synthesized by a low-temperature

hydrothermal growth through the reaction of ZnO nanowires and TAA. The formation mechanisms of the ZnO/ZnS core/shell nanorods and ZnS nanotubes are due to the sulfidation conversion and the Kirkendall effect, respectively. We have further demonstrated the successful chemical conversion of ZnS nanotubes into the other metal sulfide nanotubes such as Ag₂S, CuS, PbS, and Bi₂S₃ by the aid of the large difference in solubility. It is revealed that the yielded ZnO nanowires, ZnO/ZnS core/shell nanorods, and metal sulfide nanotubes (ZnS, Ag₂S, CuS, PbS, and Bi₂S₃) are of good crystalline structures with high optical and sensing properties. The ZnO/ZnS core/shell nanorods exhibit a distinct UV enhancement in luminescence as compared to that of the uncoated ZnO nanowires as a result of the passivated nonradiative recombination sites. Moreover, the ZnO/ZnS core/shell nanorods have much better sensitivity to H₂S than do the bare ZnO nanowires due to the improved conductance variation. Although the present work focuses on ZnO/ZnS core/shell nanorods and diverse metal sulfide nanotubes, other ZnO-based core/shell and metal sulfide hollow structures are also expected to be realized on the basis of ZnO/ZnS core/shell and ZnS hollow structures with the corresponding shapes as the precursors during the chemical conversion process. Furthermore, in addition to ZnS, other micro- and nanostructured semiconductor materials with large *K_{sp}* values can also be employed as the original reactants in the proposed chemical conversion technique. Therefore, this strategy might open up an opportunity for extensive study of the physical and chemical properties of other semiconductor core/shell and hollow structures with various compositions and morphologies, broadening their potential applications in electronics, magnetism, optics, catalysis, mechanics, electrochemistry, sensors, etc.

■ AUTHOR INFORMATION

Corresponding Author

*E-mail: wzshen@sjtu.edu.cn.

■ ACKNOWLEDGMENT

This work was supported by the National Major Basic Research Project of 2010CB933702 and the Natural Science Foundation of China under contract 10734020.

■ REFERENCES

- (1) Peng, X. G.; Schlamp, M. C.; Kadavanich, A. V.; Alivisatos, A. P. *J. Am. Chem. Soc.* **1997**, *119*, 7019.
- (2) Lee, C. C.; Chen, D. H. *Nanotechnology* **2006**, *17*, 3094.
- (3) Salgueiriño-Maceira, V.; Correa-Duarte, M. A. *Adv. Mater.* **2007**, *19*, 4131.
- (4) Deng, Y. H.; Qi, D. W.; Deng, C. H.; Zhang, X. M.; Zhao, D. Y. *J. Am. Chem. Soc.* **2008**, *130*, 28.
- (5) Toshima, N.; Shiraiishi, Y.; Shiotsuki, A.; Ikenaga, D.; Wang, Y. *Eur. Phys. J. D* **2001**, *16*, 209.
- (6) Wen, F.; Zhang, W. Q.; Wei, G. W.; Wang, Y.; Zhang, J. Z.; Zhang, M. C.; Shi, L. Q. *Chem. Mater.* **2008**, *20*, 2144.
- (7) Berndt, I.; Popescu, C.; Wortmann, F. J.; Richtering, W. *Angew. Chem., Int. Ed.* **2006**, *45*, 1081.
- (8) Shao, H. F.; Qian, X. F.; Zhu, Z. K. *J. Solid State Chem.* **2005**, *178*, 3522.
- (9) Yin, Y. D.; Rioux, R. M.; Erdonmez, C. K.; Hughes, S.; Somorjai, G. A.; Alivisatos, A. P. *Science* **2004**, *304*, 711.
- (10) Liu, B.; Zeng, H. C. *J. Am. Chem. Soc.* **2004**, *126*, 16744.

- (11) Cao, H. L.; Qian, X. F.; Wang, C.; Ma, X. D.; Yin, J.; Zhu, Z. K. *J. Am. Chem. Soc.* **2005**, *127*, 16024.
- (12) Wang, J. Z.; Loh, K. P.; Zhong, Y. L.; Lin, M.; Ding, J.; Foo, Y. L. *Chem. Mater.* **2007**, *19*, 2566.
- (13) Wang, D. B.; Song, C. X.; Hu, Z. S.; Fu, X. J. *Phys. Chem. B* **2005**, *109*, 1125.
- (14) Jang, J.; Nam, Y.; Yoon, H. *Adv. Mater.* **2005**, *17*, 1382.
- (15) Yang, Z. Z.; Niu, Z. W.; Lu, Y. F.; Hu, Z. B.; Han, C. C. *Angew. Chem.* **2003**, *115*, 1987.
- (16) Geng, J.; Liu, B.; Xu, L.; Hu, F. N.; Zhu, J. J. *Langmuir* **2007**, *23*, 10286.
- (17) Peng, Q.; Xu, S.; Zhuang, Z. B.; Wang, X.; Li, Y. D. *Small* **2005**, *1*, 216.
- (18) Gao, P. X.; Lao, C. S.; Ding, Y.; Wang, Z. L. *Adv. Funct. Mater.* **2006**, *16*, 53.
- (19) Cao, X. B.; Zhao, C.; Lan, X. M.; Gao, G. J.; Qian, W. H.; Guo, Y. J. *Phys. Chem. C* **2007**, *111*, 6658.
- (20) Chen, P.; Gu, L.; Cao, X. B. *CrystEngComm* **2010**, *12*, 3950.
- (21) Datta, A.; Panda, S. K.; Chaudhuri, S. J. *Phys. Chem. C* **2007**, *111*, 17260.
- (22) Gao, T.; Wang, T. H. *Chem. Commun.* **2004**, 2558.
- (23) Shao, H. F.; Qian, X. F.; Huang, B. C. *Mater. Lett.* **2007**, *61*, 3639.
- (24) Yi, R.; Qiu, G. Z.; Liu, X. H. *J. Solid State Chem.* **2009**, *182*, 2791.
- (25) Du, N.; Zhang, H.; Chen, B. D.; Ma, X. Y.; Liu, Z. H.; Wu, J. B.; Yang, D. R. *Adv. Mater.* **2007**, *19*, 1641.
- (26) Niu, H. J.; Gao, M. Y. *Angew. Chem., Int. Ed.* **2006**, *45*, 6462.
- (27) Wang, K. X.; Wei, M. D.; Morris, M. A.; Zhou, H. S.; Holmes, J. D. *Adv. Mater.* **2007**, *19*, 3016.
- (28) Wang, Q.; Li, J. X.; Li, G. D.; Cao, X. J.; Wang, K. J.; Chen, J. S. *J. Cryst. Growth* **2007**, *299*, 386.
- (29) Song, L. M.; Zhang, S. J.; Chen, B.; Ge, J. J.; Jia, X. C. *Colloids Surf., A* **2010**, *360*, 1.
- (30) Lubeck, C. R.; Han, T. Y.-J.; Gash, A. E.; Satcher, J. H., Jr.; Doyle, F. M. *Adv. Mater.* **2006**, *18*, 781.
- (31) Zhu, Y. F.; Fan, D. H.; Shen, W. Z. *J. Phys. Chem. C* **2008**, *112*, 10402.
- (32) Zhu, Y. F.; Fan, D. H.; Shen, W. Z. *Langmuir* **2008**, *24*, 11131.
- (33) Chen, Z. G.; Zou, J.; Liu, G.; Lu, H. F.; Li, F.; Lu, G. Q.; Cheng, H. M. *Nanotechnology* **2008**, *19*, 055710.
- (34) Yu, X. L.; Ji, H. M.; Wang, H. L.; Sun, J.; Du, X. W. *Nanoscale Res. Lett.* **2010**, *5*, 644.
- (35) Smigelskas, A. D.; Kirkendall, E. O. *Trans. AIME* **1947**, *171*, 130.
- (36) Wu, X. L.; Siu, G. G.; Fu, C. L.; Ong, H. C. *Appl. Phys. Lett.* **2001**, *78*, 2285.
- (37) Vanheusden, K.; Warren, W. L.; Seager, C. H.; Tallant, D. R.; Voigt, J. A.; Gnade, B. E. *J. Appl. Phys.* **1996**, *79*, 7983.
- (38) Duan, J. X.; Huang, X. T.; Wang, E. K.; Ai, H. H. *Nanotechnology* **2006**, *17*, 1786.
- (39) Schrier, J.; Demchenko, D. O.; Wang, L. W. *Nano Lett.* **2007**, *7*, 2377.
- (40) Shen, G. Z.; Bando, Y.; Golberg, D. *Appl. Phys. Lett.* **2006**, *88*, 123107.
- (41) Gong, J. F.; Yang, S. G.; Duan, J. H.; Zhang, R.; Du, Y. W. *Chem. Commun.* **2005**, 351.
- (42) Kumar, B.; Gong, H.; Chow, S. Y.; Tripathy, S.; Hua, Y. N. *Appl. Phys. Lett.* **2006**, *89*, 071922.
- (43) Nilsen, W. G. *Phys. Rev.* **1969**, *182*, 838.
- (44) Luo, Y. Y.; Duan, G. T.; Ye, M.; Zhang, Y. X.; Li, G. H. *J. Phys. Chem. C* **2008**, *112*, 2349.
- (45) Windischmann, H.; Mark, P. J. *Electrochem. Soc.* **1979**, *126*, 627.
- (46) Wan, Q.; Li, Q. H.; Chen, Y. J.; Wang, T. H.; He, X. L.; Li, J. P.; Lin, C. L. *Appl. Phys. Lett.* **2004**, *84*, 3654.
- (47) Weast, R. C. *CRC Handbook of Chemistry and Physics*, 69th ed.; CRC Press: Boca Raton, FL, 1988–1989.
- (48) Minceva-Sukarova, B.; Najdoski, M.; Grozdanov, I.; Chunnilal, C. J. *J. Mol. Struct.* **1997**, *410*, 267.
- (49) Krauss, T. D.; Wise, F. W.; Tanner, D. B. *Phys. Rev. Lett.* **1996**, *76*, 1376.
- (50) Smith, G. D.; Firth, S.; Clark, R. J. H.; Cardona, M. *J. Appl. Phys.* **2002**, *92*, 4375.
- (51) Krauss, T. D.; Wise, F. W. *Phys. Rev. B* **1997**, *55*, 9860.
- (52) Krauss, T. D.; Wise, F. W. *Phys. Rev. Lett.* **1997**, *79*, 5102.
- (53) Xiong, S. L.; Xi, B. J.; Xu, D. C.; Wang, C. M.; Feng, X. M.; Zhou, H. Y.; Qian, Y. T. *J. Phys. Chem. C* **2007**, *111*, 16761.
- (54) Koh, Y. W.; Lai, C. S.; Du, A. Y.; Tiekink, E. R. T.; Loh, K. P. *Chem. Mater.* **2003**, *15*, 4544.
- (55) Yang, X. H.; Wang, X.; Zhang, Z. D. *Mater. Chem. Phys.* **2006**, *95*, 154.
- (56) Wang, S. Y.; Du, Y. W. *J. Cryst. Growth* **2002**, *236*, 627.